The Canadian Mineralogist
Vol. 50, pp. 235-251 (2012)
DOI: 10.3749/canmin.50.2.235

LEAD–ANTIMONY SULFOSALTS FROM TUSCANY (ITALY). XII. BOSCARDINITE, $TlPb_4(Sb_7As_2)_{\Sigma 9}S_{18}$, A NEW MINERAL SPECIES FROM THE MONTE ARSICCIO MINE: OCCURRENCE AND CRYSTAL STRUCTURE

PAOLO ORLANDI[§], CRISTIAN BIAGIONI AND ELENA BONACCORSI

Dipartimento di Scienze della Terra, Università di Pisa, Via S. Maria 53, I–56126 Pisa, Italy

YVES MOËLO

Institut des Matériaux Jean Rouxel, UMR 6502, CNRS, Université de Nantes, 2, rue de la Houssinière, F–44 322 Nantes Cedex 3, France

WERNER H. PAAR

Department of Materials Engineering and Physics (Division of Mineralogy), University of Salzburg, Hellbrunnerstrasse 34, A–5020 Salzburg, Austria

ABSTRACT

The new mineral species *boscardinite* was discovered in the barite – pyrite – iron oxides deposit of Monte Arsiccio, near Sant'Anna di Stazzema, in the Apuan Alps, Tuscany, Italy. It forms a millimetric compact mass in a quartz vein embedded in dolomitic rocks. Other associated sulfides are stibnite and zinkenite. Boscardinite is metallic grey. Under the ore microscope, it is white; pleochroism is not discernible. Anisotropism is distinct, with an ubiquitous polysynthetic twinning; rotation tints are in shades of grey. Minimum and maximum reflectance data for COM wavelengths [λ (nm), R_{air} (%)] are: 470: 33.8/39.3, 546: 32.1/38.0, 589: 31.2/36.9, 650: 29.7/35.3. The hardness was not measured owing to the scarcity of the available material. Electron-microprobe analyses of two samples gave (wt. %, result mean of five analyses): 1) sample 4977: Ag 1.48(4), Tl 9.72(26), Pb 23.36(20), Sb 35.25(60), As 5.78(10), S 22.14(45), Se 0.04(1), total 97.77(90); 2) sample 4989: Ag 1.37(7), Tl 8.96(19), Pb 25.74(20), Sb 33.46(32), As 6.54(8), S 22.08(29), Se 0.01(1), total 98.16(63). On the basis of $\Sigma Me = 14$ *apfu*, they lead to the formulae $Ag_{0.36}Tl_{1.23}Pb_{2.92}(Sb_{7.50}As_{2.00})_{\Sigma 9.50}S_{17.88}Se_{0.01}$ and $Ag_{0.33}Tl_{1.13}Pb_{3.20}(Sb_{7.09}As_{2.25})_{\Sigma 9.34}S_{17.76}$, respectively. A single-crystal X-ray study of boscardinite indicates triclinic symmetry, space group $P\bar{1}$, with a 8.0929(4), b 8.7610(5), c 22.4971(11) Å, α 90.868(4), β 97.247(4), γ 90.793(4)°, V 1582.0(2) Å^3, $Z = 2$. The d values (Å) of the main powder-diffraction lines, corresponding to multiple *hkl* indices, are (relative intensity visually estimated): 3.705 (ms), 3.540 (ms), 3.479 (m), 3.085 (m), 2.977 (ms), 2.824 (vs), 2.707 (s), 2.324 (ms), and 2.176 (ms). Boscardinite is the Tl–Sb homeotype of baumhauerite; its crystal structure has been solved by X-ray single-crystal study on the basis of 4319 observed reflections with a final $R_1 = 0.045$. It can be described in the sartorite homologous series as formed by the 1:1 alternation of sartorite-type and dufrénoysite-type layers. The simplified structural formula is based on 18 sulfur atoms and can ideally be written as $TlPb_4(Sb_7As_2)_{\Sigma 9}S_{18}$. The name *boscardinite* honors Matteo Boscardin for his contribution to knowledge of the regional mineralogy of Italy.

Keywords: boscardinite, new mineral species, sulfosalt, thallium, lead, antimony, arsenic, Monte Arsiccio mine, Apuan Alps, Tuscany, Italy.

SOMMAIRE

La nouvelle espèce minérale *boscardinite* a été découverte dans le gisement à barite, pyrite et oxydes de fer de Monte Arsiccio, près de Sant'Anna di Stazzema, dans les Alpes Apuanes, Toscane, en Italie. Elle forme un agrégat millimétrique dans une veine de quartz au sein de dolomies. Elle est associée à stibine et zinkénite. La boscardinite est noire à éclat métallique; sous le microscope, elle paraît incolore, sans pléochroïsme visible. Son anisotropie est distincte, avec une polarisation dans les tons gris, et révèle un maclage polysynthétique ubiquiste. Les réflectances minimales et maximales aux longueurs d'onde de la COM sont [λ (nm), R_{air} (%)]: 470: 33.8/39.3, 546: 32.1/38.0, 589: 31.2/36.9, 650: 29.7/35.3. La microdureté n'a pu être mesurée du fait de la rareté du produit. L'analyse à la microsonde de deux échantillons donne (en pourcentages pondéraux, moyenne

§ *E-mail address*: orlandi@dst.unipi.it

de cinq analyses pour chaque échantillon): 1) no. 4977: Ag 1.48(4), Tl 9.72(26), Pb 23.36(20), Sb 35.25(60), As 5.78(10), S 22.14(45), Se 0.04(1), total 97.77(90); 2) no. 4989: Ag 1.37(7), Tl 8.96(19), Pb 25.74(20), Sb 33.46(32), As 6.54(8), S 22.08(29), Se 0.01(1), total 98.16(63). Sur la base de ΣMe = 14 *apfu*, les deux formules sont respectivement $Ag_{0.36}Tl_{1.23}Pb_{2.92}(Sb_{7.50}As_{2.00})_{\Sigma 9.50}S_{17.88}Se_{0.01}$ et $Ag_{0.33}Tl_{1.13}Pb_{3.20}(Sb_{7.09}As_{2.25})_{\Sigma 9.34}S_{17.76}$. L'étude aux rayons X sur monocristal donne une symétrie triclinique, groupe spatial $P\overline{1}$, avec *a* 8.0929(4), *b* 8.7610(5), *c* 22.4971(11) Å, α 90.868(4), β 97.247(4), γ 90.793(4)°, *V* 1582.0(2) Å^3, *Z* = 2. Les raies les plus intenses du diagramme des rayons X sur poudre sont (*d* en Å, intensités relatives, estimation visuelle): 3.705 (ms), 3.540 (ms), 3.479 (m), 3.085 (m), 2.977 (ms), 2.824 (vs), 2.707 (s), 2.324 (ms) et 2.176 (ms). La boscardinite est l'homéotype à Tl–Sb de la baumhauerite. Sa structure cristalline a été résolue par rayons X sur monocristal sur la base de 4319 réflexions indépendantes, avec R_1 = 0.045. C'est un membre de la série homologue de la sartorite formé de l'alternance dans un rapport 1:1 de couches de types sartorite et dufrénoysite. Sa formule structurale simplifiée, basée sur 18 atomes de soufre, est $TlPb_4(Sb_7As_2)_{\Sigma 9}S_{18}$. Le nom *boscardinite* honore Matteo Boscardin pour sa contribution à la connaissance de la minéralogie régionale italienne.

Mots-clés: boscardinite, nouvelle espèce minérale, sulfosel, thallium, plomb, antimoine, arsenic, mine de Monte Arsiccio, Alpes Apuanes, Toscane, Italie.

Introduction

The Southern Apuan Alps are characterized by the presence of small barite – pyrite – iron oxides deposits (Fig. 1); among them, the most important are those that were exploited at the Buca della Vena and the Monte Arsiccio mines. These ores are embedded either in the metavolcanic – metasedimentary sequence known as Scisti di Fornovolasco Formation, or at the contact between this formation and lenses of dolostones and marbles. Whereas the mineralogy of the Buca della Vena mine has been well known since the first description of the new oxysulfides apuanite and versiliaite (Mellini *et al*. 1979), the other barite – pyrite – iron oxides deposits of Apuan Alps have so far been neglected by mineralogists. Recently, new data were acquired on the mineralogy of the Fornovolasco mine (Biagioni *et al*. 2008, 2011) and the Monte Arsiccio mine (see below). The latter is located near the town of Sant'Anna di Stazzema and was the last barite mine to be exploited in the Apuan Alps.

Information about the geological setting and the genesis of the Monte Arsiccio ore deposit has been published by various authors (Carmignani *et al*. 1976, Cortecci *et al*. 1985, Orberger 1985, Costagliola *et al*. 1990). In these works, little attention was paid to the mineralogy of the deposit, notwithstanding the close similarity between this and the Buca della Vena mine. For this reason, a study of the mineralogy of the Monte Arsiccio mine was recently started; it allowed the identification and characterization of some rare minerals, *e.g.*, ankangite: Biagioni *et al*. (2009), benstonite: Biagioni & Orlandi (2010), chabournéite: Bonaccorsi *et al*. (2010), cymrite: Biagioni & Orlandi (2010), associated with more common species, like anatase, an apatite-group mineral, arsenopyrite, barite, dolomite, "hyalophane", pyrite, quartz, siderite, sphalerite, stibnite, tetrahedrite, valentinite, and zinkenite.

Our aim in this paper is to describe the mineral *boscardinite*, a new sulfosalt from the Monte Arsiccio mine (latitude 43°58' N, longitude 10°17' E; Fig. 1). The mineral and its name have been approved by the CNMNC–IMA, under the number 2010–079. The holotype specimen of boscardinite is deposited in the mineralogical collection of the Museo di Storia Naturale e del Territorio, Università di Pisa, Via Roma 79, Calci (PI), Italy, with catalogue number 19349. Boscardinite honors Matteo Boscardin (b. 1939), a mineral collector, for his contribution to the knowledge of regional mineralogy in Italy through the publication of over 100 papers.

Geological Setting

The barite – pyrite – iron oxides deposit of Monte Arsiccio is located in the northeastern portion of the Sant'Anna tectonic window (Fig. 1). In this area, metamorphic rocks of the Apuan and Fornovolasco–Panie units outcrop through the non-metamorphic sedimentary formations belonging to the Tuscan Nappe.

The deposit of the Monte Arsiccio mine is an almost conformable lens characterized by a distinct zoning, with pyrite + barite at the bottom, and iron oxides (magnetite and hematite) + barite at the top, with accessory sulfides and sulfosalts (Carmignani *et al*. 1976, Costagliola *et al*. 1990). The mineralization is hosted at the contact between phyllites of the Scisti di Fornovolasco Formation (belonging to the Fornovolasco–Panie Unit), probably related to the Paleozoic basement of the Apuan Unit (Pandeli *et al*. 2004), and Triassic dolostones of the Grezzoni Formation. The ore shows evidence of metamorphic deformation and recrystallization at macro- and microscopic levels. Carmignani *et al*. (1972, 1976) considered this ore deposit as the product of metasomatic replacement of carbonate rocks, genetically linked to a hypothetical synkinematic intrusive body. Owing to the absence of field evidence related to the occurrence of Tertiary magmatism along the Apuan Alps, Costagliola *et al*. (1990) proposed a different genetic model: the deposit was formed as a result of primary Triassic sedimentary–diagenetic mineralization, which was subsequently

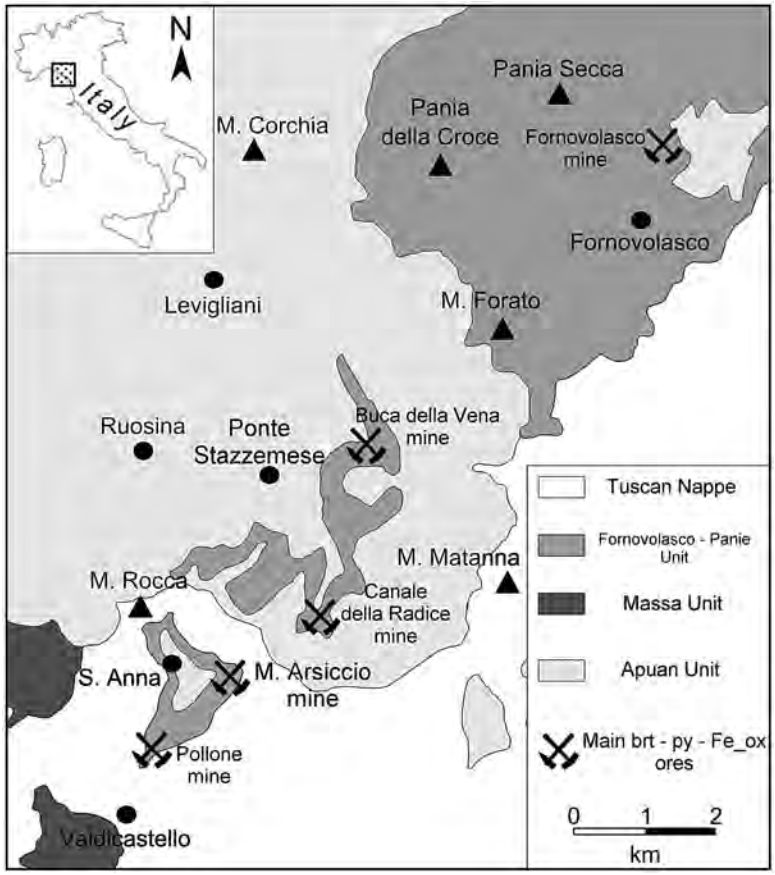

FIG. 1. The barite – pyrite – iron oxides deposits of the southern Apuan Alps, Tuscany, Italy.

metamorphosed and partly remobilized during the Tertiary Apenninic orogeny.

OCCURRENCE AND MINERAL DESCRIPTION

Boscardinite was identified in a sample collected in the Sant'Olga level (525 m a.s.l.); in the holotype specimen, it occurs in a quartz vein embedded in a dolostone, associated with zinkenite. During this study, other sulfosalts were identified in the veins cross-cutting the dolostones of the Sant'Olga level: Hg-rich "andorite", boulangerite, chabournéite, jamesonite, robinsonite, and zinkenite.

Boscardinite occurs as a millimeter-sized lead-grey mass with a metallic luster. It is brittle, with a conchoidal fracture; the streak is black. Under the ore microscope, it appears white, without internal reflections. Pleochroism is not discernible; the bireflectance is distinct. With crossed polars, the anisotropism is distinct, with rotation tints assuming different shades of grey. All crystals show a well-developed polysynthetic twinning (Fig. 2), similar to that observed in baumhauerite (Picot & Johan 1977). The reflectance has been measured in air with WTiC as a standard. Table 1 and Figure 3 give the reflectance values of boscardinite. The Vickers hardness and the density were not measured owing to the paucity of available material. On the basis of crystallographic data and the crystal-structure-based formula, the calculated density is 5.355 g/cm^3.

CHEMICAL ANALYSIS

Two fragments of boscardinite (samples 4977 and 4989) were analyzed with a CAMEBAX SX50 electron microprobe (BRGM–CNRS–University common laboratory, Orléans, France). The operating conditions were: accelerating voltage 20 kV, beam current 20 nA, beam size 5 μm. The standards (element, emission line,

counting times for one spot analysis) are: pyrite (S$K\alpha$, 20 s), stibnite (Sb$L\alpha$, 20 s), AsGa (As$L\alpha$, 30 s), Ag metal (Ag$L\alpha$, 20 s), Se element (Se$L\alpha$, 30 s), galena (Pb$M\alpha$, 20 s), lorandite (Tl$M\alpha$, 20 s).

Results of chemical analyses of the two different fragments of boscardinite analyzed are given in Table 2. Sample 4977 corresponds to the chemical formula $Ag_{0.36}Tl_{1.23}Pb_{2.92}(Sb_{7.50}As_{2.00})_{\Sigma 9.50}S_{17.88}Se_{0.01}$, whereas sample 4989 has a chemical formula $Ag_{0.33}Tl_{1.13}Pb_{3.20}(Sb_{7.09}As_{2.25})_{\Sigma 9.34}S_{17.76}$. Each of the two groups of analytical data seems to be very homogeneous.

Crystallography

The powder X-ray-diffraction pattern of boscardinite from the Monte Arsiccio mine was obtained using a Gandolfi camera 114.6 mm in diameter, with Ni-filtered Cu$K\alpha$ radiation. The observed X-ray powder pattern is compared with the calculated one (obtained using the software Powdercell: Kraus & Nolze 2000) in Figure 4 and reported in Table 3; in this table, the calculated reflections with relative intensities below 7 (over 100) were omitted, if not observed. The relative intensities of the main measured lines do not fit exactly those of the calculated ones. The discrepancies may be due to the convolution of different peaks: for example, the most intense calculated reflection should be that at 3.550 Å ($\bar{1}06$), whereas the most intense observed reflection is at 2.824 Å. Probably the superposition of at least eight different reflections around the d_{hkl} = 2.82 Å makes the intensity of this observed peak higher than that calculated. Cell parameters were not refined from the powder-diffraction data because of the multiplicity of indices for the majority of diffraction lines.

For the X-ray single-crystal study, the intensity data were collected using the sample 4977 at the CIADS (Centro Interdipartimentale di Analisi e Determinazione Strutturale) of the University of Siena (Italy), using an Oxford Xcalibur diffractometer with a Sapphire 3 CCD detector, with Mo$K\alpha$ radiation. The detector-to-crystal working distance was 45 mm. The data were corrected for the Lorentz and polarization factors; an analytical numerical-absorption correction using a multifaceted crystal model was applied (Clark & Reid 1995). The refined unit-cell parameters were obtained from 3767 reflections collected in the 2θ range 4.5–58.5°. Three datasets of 218 images were collected for 15 seconds by performing 1° ω-scans at different ϕ angles (42°, 0°, –180°, with the detector set at θ = –18°).

TABLE 1. REFLECTANCE OF BOSCARDINITE IN AIR

l (nm)	R_{min} (%)	R_{max} (%)	*l* (nm)	R_{min} (%)	R_{max} (%)
400	34.6	37.7	560	31.9	37.8
420	34.6	40.1	580	31.6	37.3
440	34.2	39.4	**589**	**31.2**	**36.9**
460	33.8	39.5	600	31.0	36.9
470	**33.8**	**39.3**	620	30.3	36.0
480	34.1	39.3	640	29.8	35.5
500	33.5	38.8	**650**	**29.7**	**35.3**
520	32.7	38.5	660	29.4	35.1
540	32.3	38.2	680	28.4	34.3
546	**32.1**	**38.0**	700	28.5	34.0

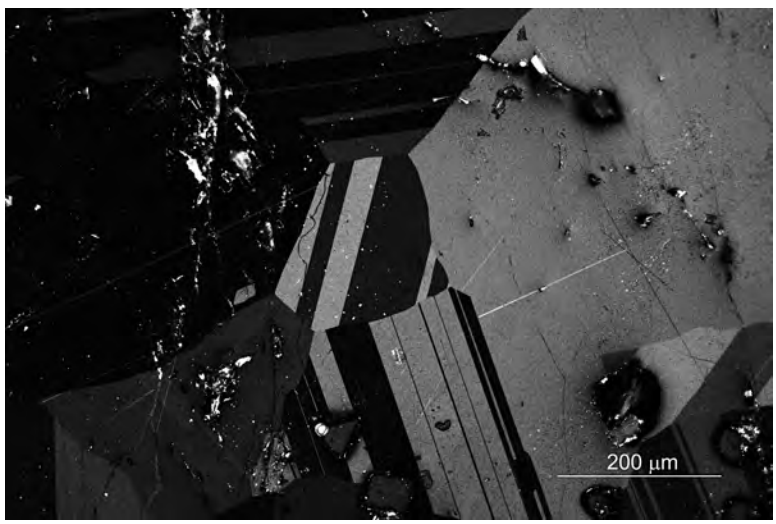

Fig. 2. Anhedral crystals of boscardinite, showing polysynthetic twinning. Reflected light, crossed polars.

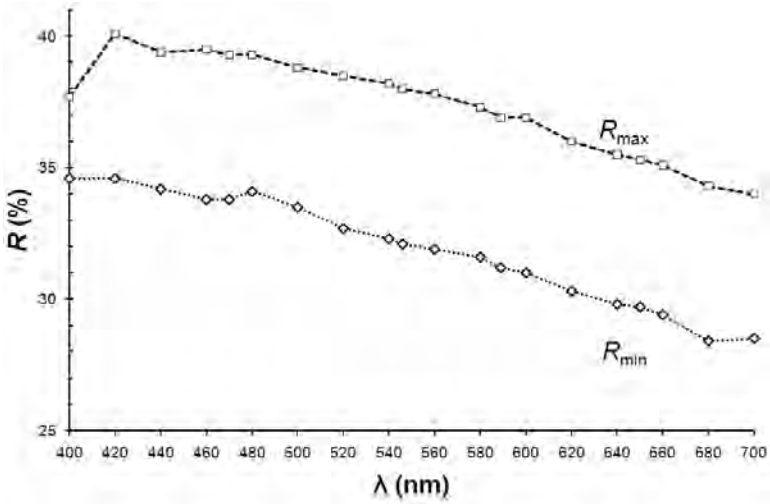

FIG. 3. Reflectance curves of boscardinite in air.

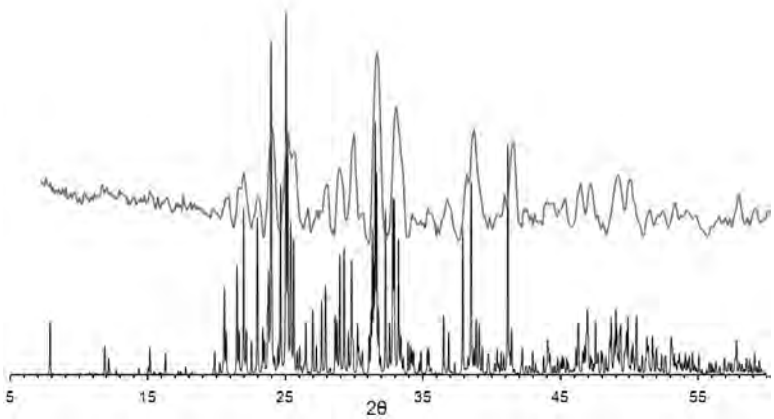

FIG. 4. Observed (grey) and calculated (black) X-ray powder diagram of boscardinite.

The refined cell parameters are *a* 8.0929(4), *b* 8.7610(5), *c* 22.4971(11) Å, α 90.868(4), β 97.247(4), γ 90.793(4)°, *V* 1582.0(2) Å^3. In order to search for a possible superstructure, a fragment of boscardinite was used to collect diffraction patterns at the Elettra synchrotron radiation facility, at Basovizza, Trieste, Italy; these patterns did not show any evidence of superstructure reflections.

The statistical tests on the distribution of |E| values ($|E^2 - 1| = 0.979$) indicate the possible presence of an inversion center. Therefore, the crystal structure was solved by direct methods using SHELXS–97 (Sheldrick 2008) in the space group $P\bar{1}$. In a first step, the maxima related to four (Pb,Tl) sites were found; successive difference-Fourier maps allowed the introduction of the remaining ten independent (Sb,As...) sites and the S sites. For more clarity, Figure 5 represents the projection of the unit cell along **b**, according to the result of the following refinement process. All atoms are on general positions (multiplicity 2). The next step was to refine the occupancy of cation sites. The (Sb,As...) sites were differentiated as four pure Sb sites, three mixed (Sb,As), one (As,Sb) sites, and two mixed sites with major Sb together with Pb or Ag. The difference-Fourier map suggested the possible splitting of these two last sites; adding these maxima and refining the structure, the *R* value dropped significantly, confirming the presence of split (Sb,Pb) and (Sb,Ag) sites, namely the Sb9a,Pb9b

and Sb10a,Ag10b pairs, respectively. For each pair, the sum of their occupancies was constrained to 1.

The last step was the filling of (Pb,Tl) sites. On the basis of the difference-Fourier map, one mixed (Pb,Tl) site was split into two subpositions, namely (Pb,Tl)2a and (Pb,Tl)2b. Owing to the very similar scattering factors of Tl and Pb, the occupancies of (Pb,Tl) sites were refined on the sole basis of bond-valence calculations (Brese & O'Keeffe 1991). For each (Pb,Tl) position, the bond-valence sum has been calculated separately for Pb and Tl, and then the Pb:Tl ratio has been adjusted in order that the bond-valence sum of the mixed position approximates the valence deduced from the Pb:Tl ratio, together with the constraints of the charge equilibrium of the final structure-based formula. As a result, the structure of boscardinite presents one pure Pb4 site, one (Pb,Tl)3, one (Tl,Pb)1, and a split one, (Pb,Tl)2a,(Pb,Tl)2b. The refinement converged to $R_1 = 0.045$ for 4319 reflections with $F_o > 4\sigma F_o$ and 0.062 for all 5855 reflections. Table 4 summarizes the crystal data and the parameters of data collection and crystal-structure refinement. Coordinates of the atoms and selected bond-distances are reported in Tables 5 and 6, respectively. A table of structure factors and a cif file are available from the Depository of Unpublished Data on the MAC website [document Boscardinite CM50_235].

TABLE 2. THE COMPOSITION OF BOSCARDINITE

Sample	4977	4989		4977	4989
Ag wt%	1.48(4)	1.37(7)	Ag *apfu*	0.36(1)	0.33(2)
Tl	9.72(26)	8.96(19)	Tl	1.23(4)	1.13(2)
Pb	23.36(20)	25.74(20)	Pb	2.92(2)	3.20(3)
Sb	35.25(60)	33.46(32)	Sb	7.50(7)	7.09(6)
As	5.78(10)	6.54(8)	As	2.00(3)	2.25(3)
S	22.14(45)	22.08(29)	S	17.88(24)	17.76(22)
Se	0.04(1)	0.01(1)	Se	0.013(5)	0.003(5)
Total	97.77(90)	98.16(63)	Ev*	0.4(1.2)	1.0(1.3)

* Relative error on valence equilibrium (%), calculated as [Σ(val+) – Σ(val-)] × 100 / Σ(val-). Data on the chemical composition were acquired with an electron microprobe and are the average result of five analyses in each case. The data are expressed in wt% on the left, and recalculated in terms of atoms per formula unit (*apfu*) on the basis of Σ*Me* = 14 *apfu*.

Crystal-Structure Description

General features

Figure 6 presents the general organization of the crystal structure. Boscardinite is homeotypic with baumhauerite (space group $P\bar{1}$ according to Le Bihan (1962), or $P1$ according to Engel & Nowacki 1969). It belongs to the sartorite homologous series (Makovicky 1985), and it can be described as formed by the 1:1 alternation, along **c**, of two layers, one of the sartorite type (N = 3), the second of the dufrénoysite type (N = 4), connected by (Pb,Tl) atoms with trigonal prismatic coordination (Fig. 5). The sartorite layer is flanked by mixed (Tl,Pb) sites, whereas the dufrénoysite layer is flanked by pure Pb and mixed (Pb,Tl) sites.

Within the layers, all sites correspond to pure Sb or mixed (Sb,As) sites, with the exception of the alternation, along **b**, in the dufrénoysite layer, of one (Sb,Pb) site with one (Sb,Ag) site. Such an equivalent (As,Pb),(As,Ag) pair in the same configuration has been described in the constitutive layer of rathite, $Ag_2Pb_{12-x}Tl_{x/2}As_{18+x/2}S_{40}$ (Berlepsch *et al.* 2002).

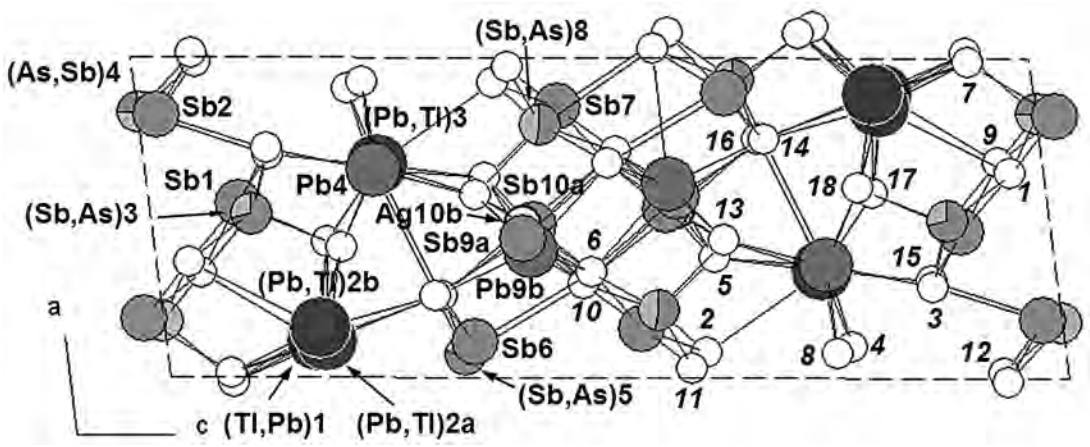

FIG. 5. Unit cell of the structure of boscardinite, as seen down [010]. In order of decreasing size: (Tl,Pb) and (Pb,Tl): grey-black, Pb: dark grey, Sb: grey, (Sb,As): site sectors grey and light grey, respectively, Ag: white with thick black border, S: white with thin border.

Cation coordination and site occupancies

Site Pb4 is occupied by Pb only. Occupancies of (Tl,Pb)1 and (Pb,Tl)3 mixed sites are $Tl_{0.80}Pb_{0.20}$ and $Pb_{0.80}Tl_{0.20}$, respectively (Table 5): the minor amount of Pb substituting for Tl in the first site equals the amount of Tl substituting for Pb in the second one. The (Pb,Tl)2a,(Pb,Tl)2b split pair has occupancies ($Pb_{0.50}Tl_{0.12}$) and ($Pb_{0.27}Tl_{0.11}$), respectively. This choice of two mixed (Pb,Tl) subpositions is the result of bond-valence calculations (Table 7). Another hypothesis would be to consider that each position corresponds either to Pb (2a) or to Tl (2b), taking into account the relative sizes of their ionic radius. This hypothesis cannot be excluded, although all the Pb present cannot be placed at a single subposition (*i.e.*, 2a). One must have in mind that not only the (Pb,Tl)2 position is split, but also potentially all S positions around it. As X-ray data do not permit to resolve such split S positions, this uncertainty prevents from refining precisely Pb,Tl partitioning between (Pb,Tl)2a and (Pb,Tl)2b subpositions.

TABLE 3. OBSERVED AND CALCULATED X-RAY POWDER-DIFFRACTION DATA FOR BOSCARDINITE

I_{meas}	d_{meas} (Å)	I_{calc}	d_{calc} (Å)	h	k	l
		15	11.16	0	0	2
vw	7.5	9	7.44	0	0	3
vw	5.8	8	5.84	1	0	1
vw	4.50					
vw	4.44	7	4.463	0	0	5
w	4.29	25	4.311	0	$\bar{2}$	1
		12	4.284	0	2	1
mw	4.11	31	4.128	$\bar{1}$	0	5
		12	4.100	0	$\bar{2}$	2
mw	4.04	47	4.040	$\bar{2}$	0	1
		12	4.004	0	$\bar{1}$	5
		10	3.938	$\bar{2}$	0	2
w	3.864	45	3.866	2	0	1
		13	3.802	0	$\bar{2}$	3
		9	3.784	1	$\bar{2}$	1
		15	3.746	0	2	3
		26	3.735	$\bar{2}$	0	3
ms	**3.705**	32	3.710	$\bar{1}$	2	2
		62	3.707	1	0	5
		17	3.699	$\bar{1}$	$\bar{2}$	2
		8	3.633	2	0	2
		55	3.606	1	$\bar{2}$	2
ms	**3.540**	100	3.550	$\bar{1}$	0	6
		63	3.533	1	2	2
		25	3.506	$\bar{1}$	$\bar{2}$	3
m	**3.479**	32	3.500	$\bar{1}$	2	3
		22	3.474	0	$\bar{2}$	4
		16	3.473	$\bar{2}$	0	4
vw	3.417	8	3.417	0	2	4
w	3.345	15	3.359	2	0	3
		18	3.298	1	2	3
w	3.265	9	3.268	$\bar{1}$	$\bar{2}$	4
		21	3.223	1	0	6
mw	3.189	20	3.192	$\bar{2}$	0	5
		8	3.188	0	0	7
		16	3.114	1	$\bar{2}$	4
		12	3.100	$\bar{1}$	0	7
m	**3.085**	34	3.079	2	0	4
		30	3.047	1	2	4
		7	3.045	1	$\bar{1}$	6
		11	3.016	$\bar{1}$	$\bar{2}$	5
		31	2.993	$\bar{1}$	2	5
ms	**2.977**	8	2.983	2	$\bar{2}$	0
		14	2.951	$\bar{2}$	$\bar{2}$	1
	2.938	7	2.942	$\bar{2}$	2	2
	2.921	6	2.918	$\bar{2}$	0	6
		11	2.872	2	2	1
		13	2.860	1	$\bar{2}$	5
		38	2.851	$\bar{2}$	2	3
vs	**2.824**	25	2.842	1	0	7
		67	2.833	$\bar{2}$	$\bar{2}$	3
		52	2.824	2	$\bar{2}$	2
		15	2.813	2	0	5
		45	2.769	2	2	2
		9	2.746	$\bar{1}$	3	1
		45	2.725	$\bar{2}$	2	4
		9	2.720	1	$\bar{1}$	7
s	**2.707**	44	2.717	$\bar{2}$	$\bar{2}$	4
		8	2.694	$\bar{1}$	3	2
		29	2.693	2	$\bar{2}$	3
		10	2.680	$\bar{3}$	0	2
		9	2.639	2	2	3
w	2.621	6	2.626	$\bar{3}$	0	3
		5	2.618	3	0	1
w	2.539	7	2.537	1	0	8
		7	2.530	3	0	2
w	2.441	17	2.458	$\bar{1}$	0	9
		12	2.435	$\bar{3}$	0	5
	2.356	40	2.371	0	$\bar{2}$	8
		13	2.338	$\bar{1}$	$\bar{2}$	8
		53	2.335	0	2	8
ms	**2.324**	12	2.314	$\bar{1}$	2	8
		14	2.302	3	0	4
		7	2.289	1	0	9
vw	2.228	6	2.230	3	2	1
w	2.204	5	2.205	$\bar{3}$	2	4
ms	**2.176**	63	2.190	0	4	0
		10	2.176	1	2	8
w	2.132	7	2.138	3	$\bar{2}$	3
vw	2.098	5	2.102	3	2	3
w	2.056	9	2.052	3	0	6
w	2.040	5	2.045	1	$\bar{2}$	9
w	1.999	5	2.007	4	0	0
mw	1.955					
mw	1.926					
mw	1.851					
mw	1.823					
w	1.775					
w	1.758					
w	1.744					
w	1.719					

Notes: the d_{hkl} values were calculated on the basis of the unit cell refined by using single-crystal diffractometer data. Intensities were calculated on the basis of the structural model. The observed intensities were visually estimated: vs: very strong, s: strong, ms: medium strong, m: medium, mw: medium weak, w: weak, and vw: very weak.

Sites (Tl,Pb)1 and (Pb,Tl)2b have a tricapped trigonal prismatic coordination, with average bond-lengths of 3.371 and 3.265 Å, respectively. The smaller size of the (Pb,Tl)2b than the (Tl,Pb)1 site is related to the preferential occupancy of the former by Pb. Bond lengths range from 2.882(6) Å with S17 to 3.693(6) Å with S1. Atom (Pb,Tl)2a has a bicapped trigonal prismatic coordination, with an average bond-length of 3.164 Å, whereas the (Pb,Tl)3 site has a monocapped trigonal prismatic coordination (with an average bond-length of 3.192 Å), with two additional longer bonds [3.699(4) and 3.792(4) Å]. Finally, the Pb4 site, occupied by Pb only, is the smallest high-coordination polyhedron in the structure of boscardinite; it has a monocapped trigonal prismatic coordination (average bond-length of 3.076 Å), with an additional longer bond of 3.557(4) Å. In the crystal structure of baumhauerite (Engel & Nowacki 1969), the sartorite and dufrénoysite layers are flanked by eight independent Pb sites (baumhauerite has a lower symmetry than boscardinite, according to these authors); these sites have average bond-lengths ranging from 3.15 to 3.24 Å and are nine-fold coordinated.

Among the ten (Sb,As...) sites, the pure Sb sites are Sb1, Sb2, Sb6, and Sb7. Atoms Sb1 and Sb2 are located in the sartorite layers, whereas the other two pure Sb sites are in the dufrénoysite layers. Considering only the Sb–S distances shorter than 3 Å, these Sb sites are four-fold-coordinated, with average bond-lengths between 2.601 (Sb1) and 2.619 Å (Sb6). If the additional longer bonds are considered, the coordination of these sites becomes VI for Sb2 and Sb6, and VII for Sb1 and Sb7. Sites (Sb,As)3, (As,Sb)4, (Sb,As)5, and (Sb,As)8 have a mixed (Sb,As) or (As,Sb) occupancy; in particular, (As,Sb)4 is the only site with As predominant over Sb, in the ratio 0.75:0.25. Sites (Sb,As)3 and (As,Sb)4 belong to the sartorite layer, whereas (Sb,As)5 and (Sb,As)8 sites belong to the dufrénoysite layer. If the (Sb,As)–S bonds shorter than 3 Å are considered, the average bond-lengths range from 2.334 Å for (As,Sb)4, in agreement with its As-rich nature, and 2.415 Å for (Sb,As)5. Taking into account also the additional bonds, the coordination number rises to VI for all these four sites.

The two remaining sites, belonging to the dufrénoysite layers, corresponds to the Sb9a,Pb9b and Sb10a,Ag10b pairs. Atoms Sb9a and Pb9b, at a distance of only 0.46 Å, exclude each other mutually. The occupancy of Sb9a,Pb9b is $Sb_{0.81}Pb_{0.19}$. Atom Sb9a is five-fold coordinated (average bond-length of 2.722 Å), with an additional bond at 3.459 Å; Pb9b occupies a monocapped trigonal prism, with bond-lengths ranging from 2.644(7) up to 3.435(7) Å. Sites Sb10a and Ag10b, at a distance of only 0.38 Å, exclude each other mutually; their refined occupancy is $Sb_{0.71}Ag_{0.29}$. Site Sb10a

TABLE 4. CRYSTAL DATA AND SUMMARY OF PARAMETERS DESCRIBING DATA COLLECTION AND THE REFINEMENT OF BOSCARDINITE

Crystal data	
X-ray formula	$Ag_{0.29}Tl_{1.23}Pb_{2.956}(Sb_{7.794}As_{1.73})_{\Sigma 9.524}S_{18}$
Crystal size (mm)	0.27 × 0.16 × 0.16
Cell setting, space group	Triclinic, $P\bar{1}$
a, *b*, *c* (Å)	8.0929(4), 8.7610(5), 22.4971(11)
α, β, γ (°)	90.868(4), 97.247(4), 90.793(4)
V (Å^3)	1582.0 (2)
Z, D_{calc} (g/cm^3)	2, 5.355
Data collection and refinement	
Radiation, wavelength (Å)	Mo*K*α, λ = 0.71073
Temperature (K)	293
Maximum observed 2θ	58.58
No. of measured reflections	7309
No. of unique reflections	5855
Reflections $F_o > 4\sigma$ (F_o)	4319
R_{int} after absorption correction	0.0243
*R*σ	0.0557
Range of *h*, *k*, *l*	$-11 \le h \le 7$, $-10 \le k \le 11$, $-24 \le l \le 28$
R [$F_o > 4\sigma F_o$]	0.0453
R (all data)	0.0622
wR (on F_o^2)	0.1137
Goof	1.000
No. of least-squares parameters	309
Maximum and minimum residual peak (*e*/Å^3)	3.26, -3.26

TABLE 5. BOSCARDINITE: POSITIONS AND EQUIVALENT DISPLACEMENT PARAMETERS OF ATOMS

Site	Occupancy	*x*	*y*	*z*	U_{eq} (Å^2)
(Tl,Pb)1	$Tl_{0.80}Pb_{0.20}$	0.11091(8)	0.63591(7)	0.16858(3)	0.0300(2)
(Pb,Tl)2a	$Pb_{0.27}Tl_{0.11}$	0.8876(7)	0.8872(4)	0.8214(2)	0.0365(5)
(Pb,Tl)2b	$Pb_{0.50}Tl_{0.12}$	0.8481(4)	0.8489(2)	0.8267(1)	0.0365(5)
(Pb,Tl)3	$Pb_{0.80}Tl_{0.20}$	0.66435(9)	0.65298(8)	0.25913(3)	0.0354(2)
Pb4	$Pb_{1.00}$	0.64766(9)	0.14848(8)	0.25445(3)	0.0357(2)
Sb1	$Sb_{1.00}$	0.5456(1)	0.3969(1)	0.09929(4)	0.0143(2)
Sb2	$Sb_{1.00}$	0.8192(1)	0.1037(1)	0.02078(4)	0.0132(2)
(Sb,As)3	$Sb_{0.71(1)}As_{0.29(1)}$	0.4867(1)	0.1174(1)	0.88652(5)	0.0147(4)
(As,Sb)4	$As_{0.75(1)}Sb_{0.25(1)}$	0.1727(2)	0.3602(1)	0.99928(6)	0.0162(4)
(Sb,As)5	$Sb_{0.78(1)}As_{0.22(1)}$	0.0685(1)	0.3880(1)	0.33165(5)	0.0153(4)
Sb6	$Sb_{1.00}$	0.1091(1)	0.8527(1)	0.34360(4)	0.0218(2)
Sb7	$Sb_{1.00}$	0.8464(1)	0.3420(1)	0.46700(5)	0.0194(2)
(Sb,As)8	$Sb_{0.53(1)}As_{0.47(1)}$	0.7884(2)	0.8996(1)	0.44625(6)	0.0230(4)
Sb9a	$Sb_{0.814(5)}$	0.4323(3)	0.1571(3)	0.4107(1)	0.0174(4)
Pb9b	$Pb_{0.186(5)}$	0.3933(7)	0.1261(7)	0.4182(3)	0.0174(4)
Sb10a	$Sb_{0.71(3)}$	0.4734(6)	0.5994(9)	0.4240(3)	0.0281(11)
Ag10b	$Ag_{0.29(3)}$	0.4768(2)	0.6311(16)	0.4128(7)	0.0281(11)
S1	$S_{1.00}$	0.3600(5)	0.1799(4)	0.0369(2)	0.0282(10)
S2	$S_{1.00}$	0.9222(4)	0.6919(4)	0.3983(2)	0.0186(8)
S3	$S_{1.00}$	0.2844(4)	0.9135(4)	0.8616(2)	0.0124(7)
S4	$S_{1.00}$	0.9030(5)	0.3872(4)	0.2359(2)	0.0242(9)
S5	$S_{1.00}$	0.6246(4)	0.3555(4)	0.3774(2)	0.0148(7)
S6	$S_{1.00}$	0.6712(4)	0.1694(4)	0.5168(2)	0.0169(8)
S7	$S_{1.00}$	0.9868(4)	0.0876(4)	0.9316(1)	0.0102(7)
S8	$S_{1.00}$	0.9233(4)	0.8812(4)	0.2532(2)	0.0179(8)
S9	$S_{1.00}$	0.3238(4)	0.5647(4)	0.0490(2)	0.0144(7)
S10	$S_{1.00}$	0.2932(4)	0.4276(4)	0.4722(2)	0.0200(8)
S11	$S_{1.00}$	0.9700(5)	0.0869(4)	0.4170(2)	0.0269(9)
S12	$S_{1.00}$	0.9849(4)	0.3314(4)	0.0704(2)	0.0143(7)
S13	$S_{1.00}$	0.5714(5)	0.9291(5)	0.3640(2)	0.0250(9)
S14	$S_{1.00}$	0.2531(4)	0.1900(4)	0.3063(2)	0.0168(8)
S15	$S_{1.00}$	0.6969(4)	0.6726(4)	0.1386(2)	0.0142(7)
S16	$S_{1.00}$	0.2542(4)	0.5991(4)	0.3128(2)	0.0184(8)
S17	$S_{1.00}$	0.4226(5)	0.3702(4)	0.1928(2)	0.0186(8)
S18	$S_{1.00}$	0.5945(5)	0.1011(4)	0.7922(2)	0.0202(8)

TABLE 6. SELECTED BOND-DISTANCES (Å) IN BOSCARDINITE

(Tl,Pb)1	- S4	3.242(4)	(Pb,Tl)2a	- S14	3.018(6)	(Pb,Tl)2b	- S17	2.880(4)	(Pb,Tl)3	- S15	2.766(4)
	- S18	3.321(4)		- S7	3.034(6)		- S12	3.009(4)		- S8	2.893(4)
	- S16	3.326(4)		- S18	3.056(7)		- S14	3.017(4)		- S4	3.126(4)
	- S8	3.353(4)		- S8	3.154(5)		- S18	3.078(5)		- S18	3.155(4)
	- S15	3.354(4)		- S12	3.196(6)		- S7	3.211(4)		- S17	3.348(4)
	- S7	3.368(3)		- S3	3.228(6)		- S4	3.327(5)		- S13	3.510(4)
	- S9	3.426(4)		- S4	3.299(7)		- S3	3.555(4)		- S2	3.545(4)
	- S17	3.454(4)		- S17	3.333(5)		- S8	3.620(4)		- S16	3.699(4)
	- S12	3.494(3)					- S1	3.691(6)		- S5	3.792(4)
Pb4	- S3	2.783(3)	Sb1	- S17	2.451(4)	Sb2	- S7	2.475(3)	(Sb,As)3	- S18	2.398(4)
	- S17	2.925(4)		- S9	2.505(4)		- S12	2.550(3)		- S15	2.410(4)
	- S4	2.990(4)		- S1	2.674(4)		- S7	2.562(3)		- S3	2.417(3)
	- S18	3.003(4)		- S15	2.774(3)		- S3	2.880(4)		- S1	3.313(4)
	- S8	3.259(4)		- S3	3.152(4)		- S1	3.048(4)		- S9	3.378(3)
	- S13	3.263(4)		- S9	3.644(4)		- S9	3.466(3)		- S1	3.691(5)
	- S5	3.312(3)		- S12	3.744(4)						
	- S14	3.557(4)									
(As,Sb)4	- S1	2.301(4)	(Sb,As)5	- S4	2.389(4)	Sb6	- S8	2.389(4)	Sb7	- S6	2.438(4)
	- S9	2.344(4)		- S14	2.413(4)		- S2	2.499(4)		- S5	2.530(3)
	- S12	2.356(4)		- S16	2.443(4)		- S16	2.651(4)		- S11	2.744(4)
	- S7	3.082(3)		- S2	3.339(4)		- S11	2.938(4)		- S10	2.755(4)
	- S12	3.333(4)		- S11	3.430(4)		- S14	3.320(4)		- S2	3.375(4)
	- S15	3.409(4)		- S10	3.454(4)		- S6	3.418(4)		- S2	3.535(4)
										- S10	3.669(4)
(Sb,As)8	- S11	2.344(4)	Sb9a	- S5	2.502(5)	Pb9b	- S13	2.644(7)	Sb10a	- S10	2.441(10)
	- S13	2.404(4)		- S13	2.580(5)		- S14	2.697(8)		- S5	2.736(6)
	- S2	2.438(4)		- S14	2.626(4)		- S5	2.961(7)		- S6	2.760(6)
	- S6	3.056(4)		- S6	2.875(4)		- S6	2.969(8)		- S10	2.826(8)
	- S11	3.430(5)		- S10	3.027(4)		- S10	3.053(7)		- S16	2.880(7)
	- S10	3.525(4)		- S6	3.459(4)		- S6	3.064(7)		- S13	3.335(11)
							- S11	3.435(7)			
Ag10b	- S16	2.707(16)									
	- S6	2.730(15)									
	- S10	2.771(15)									
	- S5	2.855(15)									
	- S13	2.975(15)									
	- S10	3.046(16)									

has a five-fold coordination (average bond-length 2.729 Å), with an additional bond at 3.335 Å. Site Ag10b is a distorted octahedron, with an average bond-length of 2.85 Å. The split sites Sb9a,Pb9b and Sb10a,Ag10b alternate along **b** in the dufrénoysite layer.

According to Table 7, the bond-valence sums of all (Sb,As...) positions are in good agreement with their valence deduced from their site occupancies.

Polymerization of (Sb,As) sites

If one considers only the shortest (= strongest) (Sb,As)–S bonds (distances below 2.70 Å), the (Sb,As) atoms present the classic triangular pyramidal coordination. The exceptions are related to the central area of the dufrénoysite layer, with split (Sb,Ag) and (Sb,Pb) positions, with only two "short" distances (Sb7), or a single one (Sb10a); it corresponds to uncertainties related to such mixed positions.

In each layer, the selection of one oblique ribbon (Fig. 6) reveals the connection of (Sb,As) atoms with closest S atoms to form $(Sb,As)_mS_n$ polymers. Figure 7 shows a central polymer $[Sb_4(As,Sb)_2]_{\Sigma 6}S_{10}$ with two lateral $(Sb,As)S_3$ groups in the sartorite layer. In the dufrénoysite layer (Fig. 8), the size of the polymer is determined by the presence or absence of Sb on the split (Sb,Pb) and (Sb,Ag) positions. The simplest polymer is $[Sb_2(Sb,As)_2]_{\Sigma 4}S_9$, whereas the longest one, all across the ribbon, is $[Sb_8(Sb,As)_4]_{\Sigma 12}S_{20}$.

Such a polymeric organization has been previously described in other Pb,(Sb,As) sulfosalts. These polymers were described as "crankshaft chains" by Berlepsch *et al*. (2001) using the example of the crystal structure of dufrénoysite. They were also recognized in sartorite (Berlepsch *et al*. 2003) and andorite VI (Sawada *et al*. 1987). As indicated by Doussier *et al*. (2008), a general trend subordinated to steric constraints is the increase of the size of the polymer [*i.e*., an increase of *m* and *n*

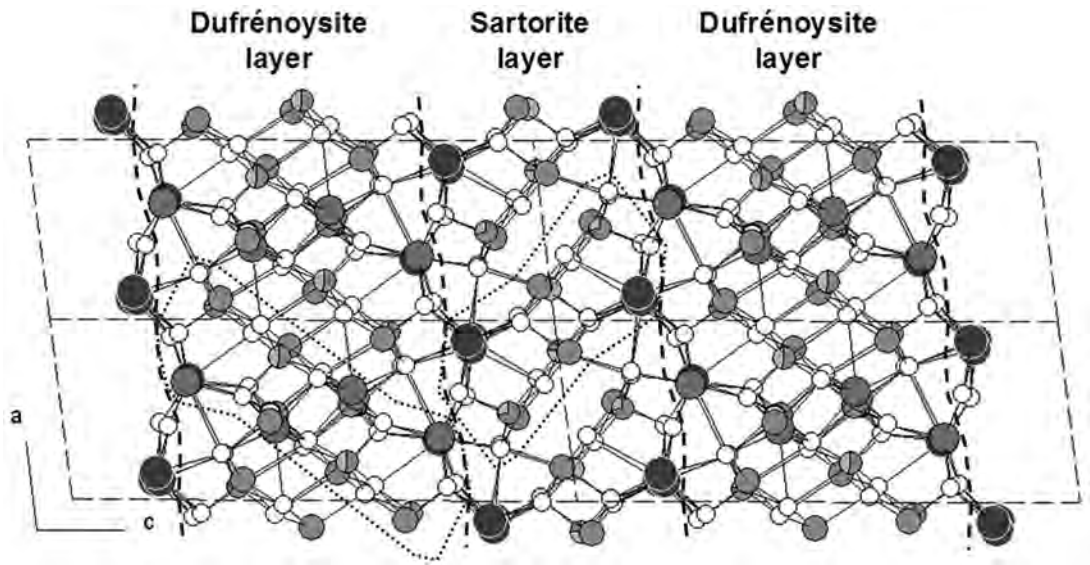

FIG. 6. Layered organization of the crystal structure of boscardinite. Two oblique ribbons have been delimited, in the sartorite layer (see Fig. 7) and the dufrénoysite layer (see Fig. 8).

TABLE 7. BOND-VALENCE CALCULATIONS FOR BOSCARDINITE

	(Tl,Pb)1	(Pb,Tl)2a	(Pb,Tl)2b	(Pb,Tl)3	Pb4	Sb1	Sb2	(Sb,As)3	(As,Sb)4	(Sb,As)5	Sb6	Sb7	(Sb,As)8	Sb9a	Pb9b	Sb10a	Ag10b	Σ_{anions}
S1			0.03			0.55	0.20	0.12	1.05									1.95
S2				0.07						0.08	0.88	0.13	0.84					2.00
S3		0.07	0.04		0.53	0.15	0.31	0.97										2.07
S4	0.18	0.05	0.08	0.22	0.30	0.04				1.08								1.95
S5				0.04	0.13							0.81		0.70	0.06	0.33	0.04	2.11
S6											0.07	1.03	0.16	0.31	0.11	0.31	0.06	2.05
S7	0.13	0.11	0.11				1.67		0.13									2.15
S8	0.14	0.08	0.04	0.41	0.15						1.18							2.00
S9	0.11					0.86	0.06	0.07	0.93									2.03
S10										0.06		0.48	0.04	0.17	0.05	0.99	0.08	1.87
S11										0.06	0.27	0.45	1.14		0.02			1.94
S12	0.09	0.07	0.19				0.76		0.96									2.07
S13				0.08	0.15								0.92	0.57	0.15	0.07	0.03	1.97
S14		0.11	0.18		0.07					1.01	0.10			0.51	0.13			2.11
S15	0.15			0.59		0.42		0.98	0.05									2.19
S16	0.15			0.05						0.93	0.58					0.22	0.06	1.99
S17	0.10	0.05	0.27	0.12	0.36	1.00												1.90
S18	0.15	0.10	0.16	0.20	0.29			1.02										1.92
$\Sigma_{cations}$	1.20	0.64	1.10	1.78	1.98	3.02	3.00	3.16	3.12	3.22	3.08	2.90	3.10	2.26	0.52	1.91	0.27	
Theor.*	1.20	0.65	1.12	1.80	2.00	3.00	3.00	3.00	3.00	3.00	3.00	3.00	3.00	2.44	0.37	2.13	0.29	

In mixed sites, bond-valence contribution of each cation has been weighted according to its occupancy (see Table 5). * Theoretical valence on the basis of site occupancies. Bond valences, expressed in valence units (*vu*), are calculated according to the constants of Brese & O'Keeffe (1991).

coefficients in the formula $(Sb,As)_mS_n$] with an increase of the Sb:As ratio.

Crystal Chemistry of Boscardinite

Structural formula

The crystal-chemical formula obtained through crystal-structure refinement is $Ag_{0.29}Tl_{1.23}Pb_{2.956}(Sb_{7.794}As_{1.73})_{\Sigma 9.524}S_{18}$, in agreement with the formula obtained through chemical analysis.

This structural formula can be reduced to a stoichiometric one taking into account the fragment of the structure in which are located mixed or split sites with different valence states (Fig. 9). This fragment deals with the dufrénoysite layer and the (Pb,Tl) positions at the junction between the two types of layers. There are six (× 2) mixed or split sites, with the resulting composition $Ag_{0.29}Tl_{1.23}Pb_{2.956}Sb_{1.524}$ (1), and a valence total equal to 12.004, ideally 12. The four sites at the layer junction correspond to $Tl_{1.23}Pb_{2.77}$ (2), which can be simplified as $TlPb_3$. The two (Sb,Pb) and (Sb,Ag) split sites correspond to $Ag_{0.29}Pb_{0.186}Sb_{1.524}$. This last formula, through the elimination of Ag according to $Ag^+ + Sb^{3+} \rightarrow 2\ Pb^{2+}$, becomes $Pb_{0.766}Sb_{1.234}$ (3), which can be simplified as PbSb. The valence deficit of (2) is compensated by the valence excess of (3), and corresponds to the substitution rule $Tl^+ + Sb^{3+} \rightarrow 2\ Pb^{2+}$. The simplified stoichiometric formula derived from (1) is thus $TlPb_4Sb$; for the whole structure, one obtains the formula $TlPb_4(Sb_{7.28}As_{1.72})_{\Sigma 9}S_{18}$, ideally $TlPb_4(Sb_7As_2)_{\Sigma 9}S_{18}$. On this basis, the generalized formula, taking into account the three possible chemical substitutions, is: $Ag_xTl_{1+y}Pb_{4-2x-2y}(Sb_{7+x+y+z}As_{2-z})_{\Sigma 9+x+y}S_{18}$, with $x \approx 0.29$, $y \approx 0.23$, and $z \approx 0.28$ for the fragment of sample 4977 studied by single-crystal X-ray diffraction. On the basis of electron-microprobe results, the coefficients x, y, and z are ~0.33, ~0.23, and ~0, respectively, for sample 4977, and ~0.36, ~0.13, and ~–0.25 for sample 4989.

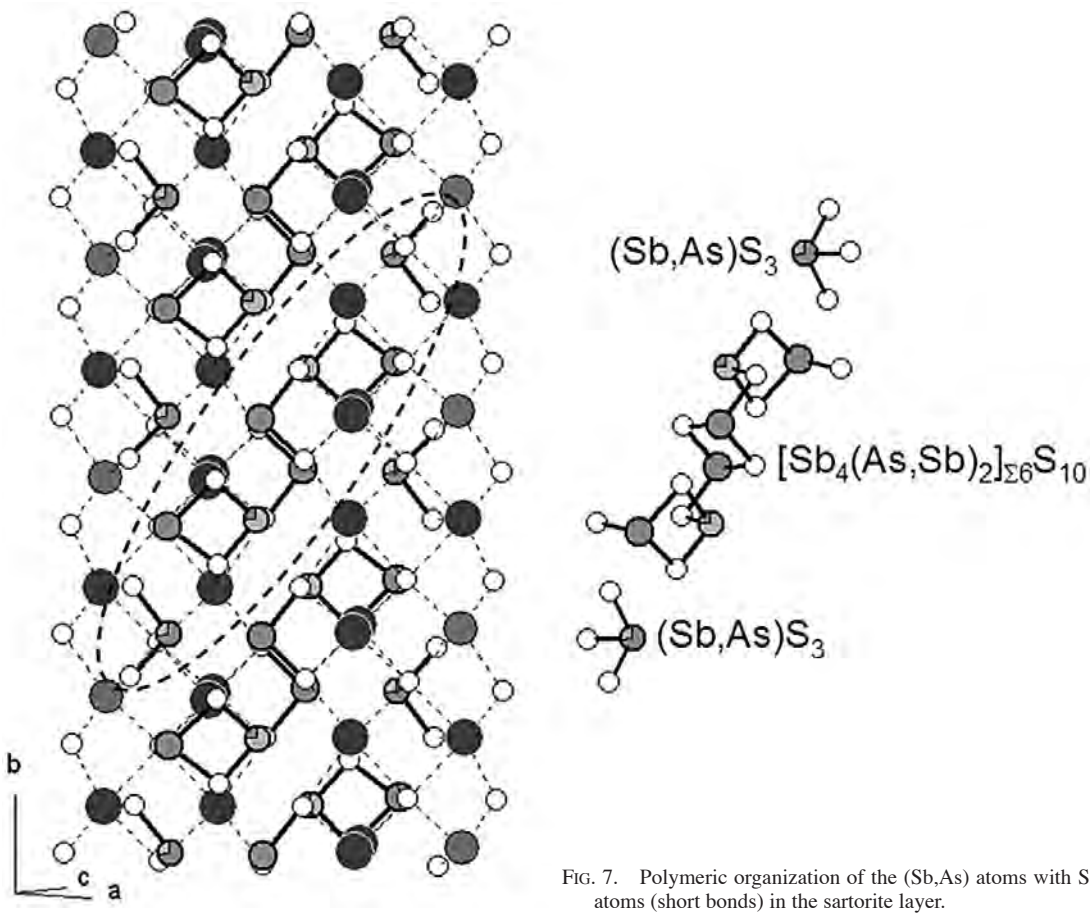

FIG. 7. Polymeric organization of the (Sb,As) atoms with S atoms (short bonds) in the sartorite layer.

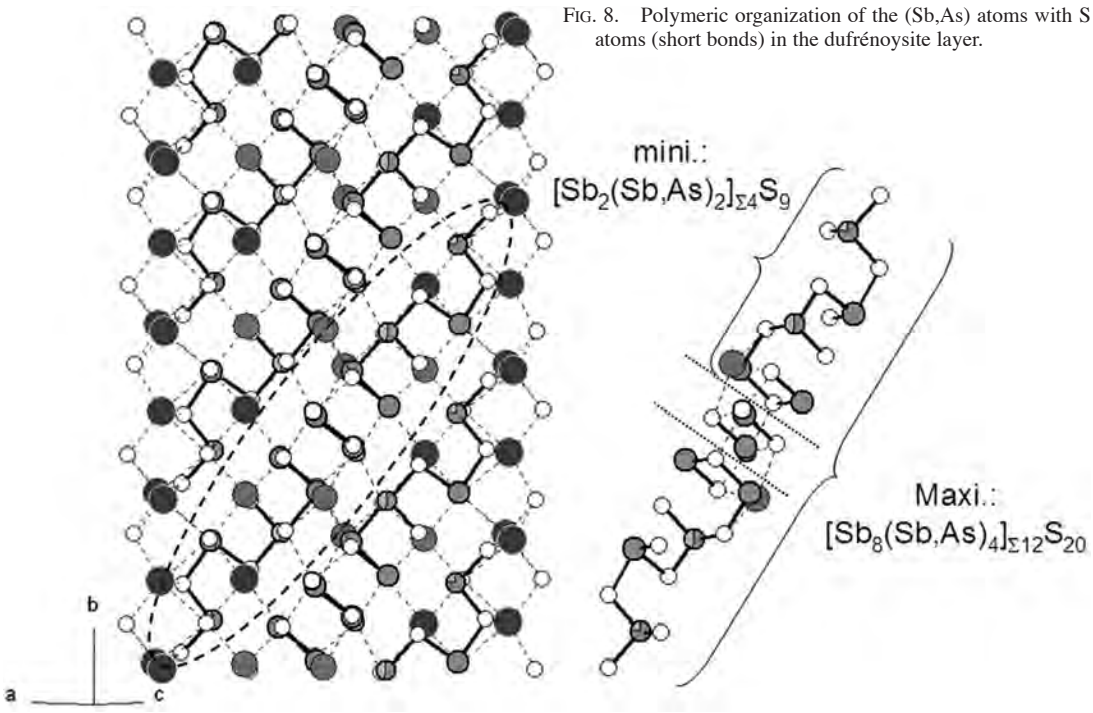

FIG. 8. Polymeric organization of the (Sb,As) atoms with S atoms (short bonds) in the dufrénoysite layer.

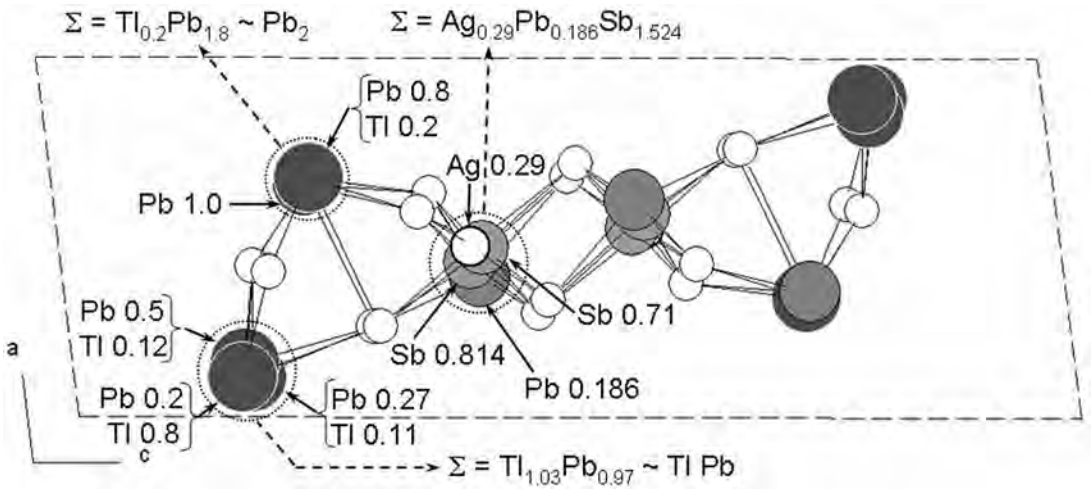

FIG. 9. Fragment of the structure (related to the dufrénoysite layer) with mixed or split cation sites with distinct valence states.

The ideal formula of boscardinite agrees with the general formula for members of the sartorite homologous series, $(Tl,Ag)^{+}_{x}Pb^{2+}_{4N-8-2x}(As,Sb)^{3+}_{8+x}S^{2-}_{4N+4}$ (Makovicky 1985), with $x = 1$ and N = 3.5.

Another crystal-chemical peculiarity of the structure is the partitioning of Sb and As between the two types of layer. In the sartorite layer, the Sb:As atomic ratio is 2.968/1.032 = 2.876; in the dufrénoysite layer, this ratio is 4.835/0.689 = 7.017. Thus, the sartorite layer, which

presents the only mixed (As,Sb) site with major As, and is flanked by prismatic sites with major Tl, concentrates As relative to the dufrénoysite layer, flanked by prismatic sites with major Pb. This emphasizes the steric affinity between Tl and As.

Silver in the sartorite series

The dufrénoysite layer of boscardinite also hosts Ag. This element has been observed in variable amounts in some members of the sartorite homologous series (Table 8). Engel & Nowacki (1969) solved the crystal structure of a sample of Ag-bearing baumhauerite, which appeared to correspond to a specific mineral observed later in intergrowth with "true" Ag-free baumhauerite (Laroussi *et al*. 1989), and defined as the species baumhauerite-2*a* by Pring *et al*. (1990). Laroussi *et al*. (1989) thus considered that Ag played a decisive role for the stabilization of this species (as well as rathite), which was explained on the basis of crystal-structure studies by cation ordering (Pring *et al*. 1990, Pring & Graeser 1994, Pring 2001).

Table 8 shows that the Ag content of boscardinite is the same as in baumhauerite-2*a*. The Ag content of liveingite is lower, and does not seem to indicate the existence of a specific Ag homeotypic derivative, according to Laroussi *et al*. (1989). On the contrary, rathite presents a significant Ag content (about two atoms in the formula unit), and the peculiar crystal-chemical role of this metal, which distinguishes rathite from dufrénoysite, was underlined by the crystal-structure study of rathite-I by Marumo & Nowacki (1965), then confirmed by new electron-microprobe analyses (Laroussi *et al*. 1989). Berlepsch *et al*. (2002) studied the importance of the heterovalent substitution $Ag^{+} + As^{3+} = 2\ Pb^{2+}$ for the stability of the rathite structure. The crystal structure of this sulfosalt can be described as formed by chemically twinned layers of dufrénoysite. Taking into account the parent structure suggested by Pring (2001), having space group *Pmnb* and unit-cell parameters *a* 4.23, *b* 7.92, and *c* 24.7 Å, Berlepsch *et al*. (2002) showed that this structure is not stable for the composition $Pb_{16}As_{16}S_{40}$ because of the requirements of bond-valence balance at the atom scale. In particular, they focused their attention on the $S4_{Pmnb}$ site, which is strongly overbonded. This site corresponds, in the crystal structure of rathite, to $S3_r$ and $S4_r$; the Ag,As and Pb,As substitutions are essential in reducing the oversaturation of these sulfur sites.

The dufrénoysite layer occurring in boscardinite is quite similar to that of rathite, with the difference related to the occurrence of Sb^{3+} instead of As^{3+}. In the boscardinite structure, $S4_{Pmnb}$ of rathite is separated into the two symmetry-independent $S14_{bos}$ and $S16_{bos}$ sites. Atom $S14_{bos}$ is bonded to one SbS_3 trigonal pyramid [(Sb,As)5], two nine-fold-coordinated (Pb,Tl) sites [(Pb,Tl)2a,(Pb,Tl)2b and Pb4] and either of the split Sb9a,Pb9b sites; S16b bonds two SbS_3 pyramids [(Sb,As)5, Sb6], two nine-fold-coordinated (Pb,Tl) sites [(Tl,Pb)1 and (Pb,Tl)3], and either of the split Sb10a,Ag10a sites. An important difference between the situations described for rathite and those in boscardinite is related to the presence of Tl in the latter. In fact, the oversaturation of S is reduced also by the substitution of Tl^{+} for Pb^{2+}.

TABLE 8. Ag IN HOMOLOGUES OF THE SARTORITE SERIES

	Unit formula	Source
	Baumhauerite-2*a* (N = 3.5)	
STR, EMP	$Ag_{0.6}Pb_{11.6}As_{15.7}S_{36}$	Engel & Nowacki (1969)
EMP	$Ag_{0.65}Tl_{0.10}Pb_{10.54}As_{16.68}S_{36}$	Laroussi *et al.* (1989)
STR, EMP	$Ag_{0.7}Pb_{11}Sb_{0.4}As_{17.2}S_{36}$	Pring *et al.* (1990)
	Boscardinite (N = 3.5)	
STR	$Ag_{0.58}Tl_{2.46}Pb_{5.92}Sb_{15.60}As_{3.44}S_{36}$	This study
EMP No. 4977	$Ag_{0.66}Tl_{2.46}Pb_{5.76}Sb_{15.12}As_{4.00}S_{36}$	This study
EMP No. 4989	$Ag_{0.72}Tl_{2.28}Pb_{6.04}Sb_{14.48}As_{4.50}S_{36}$	This study
	Liveingite (N = 3.67)	
EMP	$Ag_{0.33}Tl_{0.19}Pb_{18.75}As_{24.73}S_{56}$	Laroussi *et al.* (1989)
	Rathite (4)	
STR, EMP	$Ag_{2.3}Tl_{0.9}Pb_{11.1}As_{17.6}S_{40}$	Marumo & Nowacki (1965)
EMP	$Ag_{1.88}Tl_{0.36}Pb_{11.36}Sb_{0.14}As_{19.10}S_{40}$	Laroussi *et al.* (1989)
EMP*	$Ag_{1.97}Tl_{1.17}Pb_{9.55}Sb_{1.01}As_{18.59}S_{40}$	Berlepsch *et al.* (2002)
STR	$Ag_{1.90}Pb_{10.96}Sb_{1.06}As_{18.09}S_{40}$	Berlepsch *et al.* (2002)

STR: crystal structure, EMP: microprobe analysis. * Mean of 4 analyses.

Discussion

Systematics of Tl–Pb sulfosalts and relationship with other species

Boscardinite is the second thallium sulfosalt described from the Apuan Alps, in Tuscany, and the tenth natural Tl–Pb sulfosalt (Table 9). Boscardinite is the Tl–Sb analogue (homeotype) of baumhauerite; in fact, relative to baumhauerite, $Pb_6As_8S_{18}$, the two significant chemical differences are Sb over As, and the presence of a Tl site and mixed (Pb,Tl) sites, with major Pb. A sample of Sb-rich baumhauerite was described by Jambor (1967) from Madoc, Ontario; this author reported results of two electron-microprobe analyses, corresponding to the chemical formulae $Pb_{5.93}(As_{4.27}Sb_{3.80})_{\Sigma 8.07}S_{17.15}$ and $Pb_{5.84}(As_{4.08}Sb_{4.08})_{\Sigma 8.16}S_{16.68}$, based on $\Sigma Me = 14$ atoms per formula unit. These two formulae, which show an excess of positive charges owing to a deficiency of S atoms, have a As:Sb ratio close to 1, the lowest measured in baumhauerite specimens.

In Table 10, we compare the unit-cell parameters of boscardinite with those of the other members of the baumhauerite homeotypic group, *i.e.*, baumhauerite and baumhauerite-2*a*. In comparison to these two species, the *a* and *b* cell parameters are larger, owing to the introduction of Tl and Sb, relatively to Pb and As.

In the systematic review of sulfosalts (Moëlo *et al.* 2008), boscardinite belongs to the sartorite homologous series (group no. 3.8). On the other hand, hutchinsonite, $TlPbAs_5S_9 \times 2 = Tl_2Pb_2As_{10}S_{18}$, edenharterite, $TlPbAs_3S_6 \times 3 = Tl_3Pb_3As_9S_{18}$, and its isotypic derivative jentschite, $TlPbAs_2SbS_6 \times 3 = Tl_3Pb_3As_6Sb_3S_{18}$, which have similar chemical formulae but distinct crystal structures, belong to the group no. 5.1 of the hutchinsonite merotypic series (Makovicky 1997). Relatively to baumhauerite, $Pb_6As_8S_{18}$, the incorporation of Tl in boscardinite through the substitution $2\ Pb^{2+}$ for $Tl^+ + As^{3+}$ would favor a structural evolution toward a hutchinsonite derivative, but apparently such a change is prevented by the replacement of As by major Sb.

Boscardinite and the regional metallogeny of Tl

With the description of the new mineral species boscardinite and the occurrence of chabournéite (Bonaccorsi *et al.* 2010), the Monte Arsiccio mine is now the second Italian locality showing the presence of thallium-bearing mineral assemblages, after the magmatic hydrothermal system of the La Fossa crater on Vulcano, Aeolian Islands, Sicily, Italy (Campostrini *et al.* 2011). However, whereas in the latter thallium is not usually present in sulfides and sulfosalts, preferentially forming halides, Monte Arsiccio mine has become an interesting locality for the study of thallium sulfosalts in a metamorphic environment.

It is interesting to note that notwithstanding over two centuries of mineralogical studies on the Apuan Alps ores, only recently was the first thallium mineral identified (chabournéite from the Monte Arsiccio mine; Bonaccorsi *et al.* 2010). At the same time, Moëlo *et al.* (2011) detected the presence of Tl in Sb-rich sterryite from the Pollone mine, confirming the geochemical complexity of the hydrothermal paragenesis of the barite – pyrite – (iron oxides) deposits in the Apuan Alps.

Thallium is a rare element; the average concentration in the Earth's crust is 0.4–0.6 ppm (Reimann & de Caritat 1998), with the most abundant reservoir represented by calc-alkaline granites (10.72 ppm; Faure 1991). However, it is noteworthy that the most important thallium deposits, *i.e.*, the Lanmuchang Hg–Tl deposit, in Ghizou Province, China, and the

TABLE 9. Tl–Pb SULFOSALTS KNOWN IN NATURE

Mineral	Chemical formula	*a* (Å)	*b* (Å)	*c* (Å)	α (°)	β (°)	γ (°)	S.G.	Ref.
Chabournéite	$Tl_{5-x}Pb_{2x}(Sb,As)_{21-x}S_{34}$	16.346	42.602	8.534	95.86	86.91	96.88	*P*1	(1)
Dalnegroite	$Tl_{5-x}Pb_{2x}(As,Sb)_{21-x}S_{34}$	16.217	42.544	8.557	95.72	90.25	96.78	*P*1	(2)
Edenharterite	$TlPbAs_3S_6$	15.465	47.507	5.843				*Fdd*2	(3)
Hatchite	$AgTlPbAs_2S_5$	9.22	7.84	8.06	66.42	65.28	74.90	$P\bar{1}$	(4)
Hutchinsonite	$TlPbAs_2S_9$	10.786	35.389	8.141				*Pbca*	(5)
Jentschite	$TlPbAs_2SbS_9$	8.121	23.969	5.847		107.68		$P2_1/n$	(6)
Rathite	$Ag_2Pb_{12-x}Tl_{x/2}As_{18+x/2}S_{40}$	8.496	7.969	25.122		100.704		$P2_1/c$	(7)
Rayite	$(Ag,Tl)_2Pb_8Sb_8S_{21}$	13.60	11.96	24.49		103.94		UK	(8)
Wallisite	$CuTlPbAs_2S_5$	8.98	7.76	7.98	65.55	65.50	73.92	$P\bar{1}$	(9)
Boscardinite	$TlPb_4Sb_7As_2S_{18}$	8.09	8.76	22.50	90.87	97.25	90.79	$P\bar{1}$	(10)

(1) Johan *et al.* (1981), (2) Nestola *et al.* (2009), (3) Graeser & Schwander (1992), (4) Marumo & Nowacki (1967), (5) Matsushita & Takéuchi (1994), (6) Graeser & Edenharter (1997), (7) Berlepsch *et al.* (2002), (8) Basu *et al.* (1983), (9) Takéuchi *et al.* (1968), (10) this study. Notations: UK: unknown, S.G.: space group.

TABLE 10. CELL PARAMETERS OF BAUMHAUERITE AND HOMEOTYPIC DERIVATIVES

Mineral	Chemical formula	*a* (Å)	*b* (Å)	*c* (Å)	α (°)	β (°)	γ (°)	S.G.	Ref.
Baumhauerite	$Pb_5As_9S_{18}$	22.78	8.33	7.90	90	97.4	90	$P\bar{1}$	(1)
Baumhauerite	$Pb_{12}As_{16}S_{36}$	7.894	8.357	22.80	89.92	97.26	90.05	*P*1	(2)
Baumhauerite-2*a*	$Ag_{0.7}Pb_{11}As_{17.2}Sb_{0.4}S_{36}$	7.91	8.477	44.74		93.37		UK	(3)
Boscardinite	$Tl_2Pb_8Sb_{14}As_4S_{36}$	8.093	8.761	22.50	90.87	97.25	90.79	$P\bar{1}$	(4)

(1) Le Bihan (1962), (2) Engel & Nowacki (1969), (3) Pring *et al.* (1990), (4) this study. Notations: UK: unknown, S.G.: space group.

Allchar Sb–As–Tl–Au ore, in Macedonia, are hosted by carbonate-bearing formations (average thallium content in carbonates: 0.01 ppm; Faure 1991). Other well-known thallium-rich assemblages are those of Lengenbach, Binntal, Switzerland (Hofmann & Knill 1996) and Jas Roux, Hautes-Alpes, France (Johan & Mantienne 2000). As suggested by Xiong (2007), carbonate rocks could provide a favorable environment for the deposition of thallium, because carbonates neutralize acidic solutions (thallium is more soluble in low-pH solutions) and buffer them to neutral to mildly alkaline pH. The occurrence of thallium sulfosalts at the Monte Arsiccio mine is limited to a carbonate lens embedded in schists; in particular, they occur in the pyrite ores, at the footwall of the carbonate lens, or in quartz–barite–carbonate veins. The first occurrence of boscardinite described here was noted in a quartz vein embedded in the dolostone; then, new samples (under study) were found as mm-sized veins cross-cutting a pyrite-rich dolostone, together with chabournéite, routhierite, and stibnite. Therefore, hydrothermal solutions transporting thallium were probably neutralized by carbonate rocks, promoting the deposition of thallium-bearing phases.

The source of thallium in the Apuan Alps ores is still unknown. Geochemical data about the Tl content in the rocks of Apuan Alps are missing. As stated above, the most Tl-rich rocks are represented by calc-alkaline granitic rocks; the enrichment of Tl in the latest stages of the magmatic differentiation is in agreement with the similarity of its behavior with K and Rb. In the Apuan Alps, felsic magmatism is confined to the Ordovician calc-alkaline metavolcanic rocks belonging to the Porfiroidi Formation; according to Pandeli *et al*. (2004), the Scisti di Fornovolasco Formation is correlated with the Filladi inferiori and Porfiroidi and Scisti porfirici formations of the Apuane Unit. Therefore, hydrothermal leaching of thallium from the Paleozoic basement could be the source for the precipitation of Tl sulfosalts at Monte Arsiccio.

Hofmann & Knill (1996) stated that the association of Pb–As–Tl–Cu–Hg–Sb–Ba is typical of hydrothermal fluids derived from evolved continental crust, and that it is found in Kuroko-type and sediment-hosted massive sulfides, in epithermal systems, and high-temperature fluids. This could be the case for the Monte Arsiccio Ba–Fe–Pb–Zn–Cu–Sb–As–Tl–Hg ore. High concentrations of lead and thallium were found, for example, in pyrite from the Meggen sediment-hosted sulfide deposit in Germany (Gasser & Thein 1977) and in Belgian lead–zinc vein deposits (Duchesne *et al*. 1983). Also in this case, however, geochemical data about pyrite from Apuan Alps are lacking. Further studies will be necessary to unravel the actual source of thallium.

Summary and Conclusions

Boscardinite is a new sulfosalt species, the (Tl,Sb)-rich homeotypic derivative of baumhauerite, within the sartorite homologous series. Its crystal chemistry brings useful new data for the knowledge of phase equilibria in the system $PbS–Tl_2S–As_2S_3–Sb_2S_3$. An interesting question will be to define the limit between Sb-rich baumhauerite and its homeotype boscardinite.

The descriptions of chabournéite and boscardinite, as well as other mineralogical studies in progress, indicate that the Monte Arsiccio mine presents a high potential for the mineralogy of sulfosalts, owing to its complex geochemistry (Pb, Sb, As, Tl, Ag, Hg, Cu, Zn...). Such a geochemistry relates the Monte Arsiccio mine to other famous deposits of complex sulfosalts, among which Binn in Switzerland, Madoc in Canada, and Jas Roux in France are the best representatives.

Acknowledgements

Electron-microprobe analyses were performed with the help of O. Rouer (CNRS engineer, Institut des Sciences de la Terre d'Orléans). We are grateful to mineral collector Riccardo Mazzanti for providing us with the first specimen of boscardinite. Gerald Giester and an anonymous referee, the associate editor Tonci Balić-Žunić, and Prof. Robert Martin are warmly thanked for their constructive revision of the paper.

Since 2000, many new lead sulfosalts have been discovered in the Apuan Alps (scainiite, pillaite, pellouxite, rouxelite, marrucciite, parasterryite, boscardinite), and their crystal structure has been solved. Such a detailed crystal chemical work would have not been possible without the powerful system developed by Professor Emil Makovicky for the modular analysis of the crystal structures of sulfosalts. We are greatly indebted to him for his fundamental work, as well as for his friendly advice and comments throughout all these studies.

References

Basu, K., Bortnikov, N.S., Moorkherjee, A., Mozgova, N.N., Tsepin, A.I. & Vyalsov, L.N. (1983): Rare minerals from Rajpura–Dariba, Rajasthan, India. IV. A new Pb–Ag–Tl–Sb sulfosalt, rayite. *Neues Jahrb. Mineral., Monatsh.*, 296-304.

Berlepsch, P., Armbruster, T., Makovicky, E. & Topa, D. (2003): Another step toward understanding the true nature of sartorite: determination and refinement of a ninefold superstructure. *Am. Mineral.* **88**, 450-461.

Berlepsch, P., Armbruster, T. & Topa, D. (2002): Structural and chemical variations in rathite, $Pb_8Pb_{4-x}(Tl_2As_2)_x(Ag_2As_2)As_{16}S_{40}$: modulations of a parent structure. *Z. Kristallogr.* **217**, 581-590.

Berlepsch, P., Makovicky, E. & Balić-Žunić, T. (2001): Crystal chemistry of the sartorite homologues and related sulfosalts. *Neues Jahrb. Mineral., Abh.* **176**, 45-66.

BIAGIONI, C., BONACCORSI, E. & ORLANDI, P. (2011): Volaschioite, $Fe^{3+}_4(SO_4)O_2(OH)_6•2H_2O$, a new mineral from Fornovolasco, Apuan Alps, Tuscany (Italy). *Can. Mineral.* **49**, 605-614.

BIAGIONI, C. & ORLANDI, P. (2010): Cymrite and benstonite from the Monte Arsiccio mine (Apuan Alps, Tuscany, Italy): first Italian occurrence. *Plinius* **36**, 365.

BIAGIONI, C., ORLANDI, P. & BONINI, M. (2008): Fornovolasco. Storia e miniere di ferro presso Vergemoli (Alpi Apuane). *Riv. Mineral. Ital.* **32**, 230-252.

BIAGIONI, C., ORLANDI, P. & PASERO, M. (2009): Ankangite from the Monte Arsiccio mine (Apuan Alps, Tuscany, Italy): occurrence, crystal structure, and classification problems in cryptomelane group minerals. *Per. Mineral.* **78**, 3-11.

BONACCORSI, E., BIAGIONI, C., MOËLO, Y. & ORLANDI, P. (2010): Chabournéite from Monte Arsiccio mine (Apuan Alps, Tuscany, Italy): occurrence and crystal structure. *Int. Mineral. Assoc., 20th Gen. Meeting* (*Budapest*), *Abstr. Ser.* **6**, 714.

BRESE, N.E. & O'KEEFFE, M. (1991): Bond-valence parameters for solids. *Acta Crystallogr.* **B47**, 192-197.

CAMPOSTRINI, I., DEMARTIN, F., GRAMACCIOLI, C.M. & RUSSO, M. (2011): *Vulcano. Tre secoli di mineralogia*. Associazione Micro-mineralogica Italiana, Cremona, Italy.

CARMIGNANI, L., DESSAU, G. & DUCHI, G. (1972): I giacimenti minerari delle Alpi Apuane e loro correlazione con l'evoluzione del gruppo montuoso. *Mem. Soc. Geol. Ital.* **11**, 417-431.

CARMIGNANI, L., DESSAU, G. & DUCHI, G. (1976): I giacimenti a barite, pirite ed ossidi di ferro delle Alpi Apuane. Studio minerogenetico e strutturale. *Boll. Soc. Geol. Ital.* **95**, 1009-1061.

CLARK, R.C. & REID, J.S. (1995): The analytical calculation of absorption in multifaceted crystals. *Acta Crystallogr.* **A51**, 887-897.

CORTECCI, G., LATTANZI, P. & TANELLI, G. (1985): Barite–iron oxides-pyrite deposits from the Apuane Alps, northern Tuscany, Italy. *Mem. Soc. Geol. Ital.* **30**, 337-345.

COSTAGLIOLA, P., BENVENUTI, M., LATTANZI, P. & TANELLI, G. (1990): The barite–pyrite–iron oxides deposit of Monte Arsiccio (Apuane Alps). Geological setting, mineralogy, fluid inclusions, stable isotopes and genesis. *Boll. Soc. Geol. Ital.* **109**, 267-277.

DOUSSIER, C., MOËLO, Y., LÉONE, P., MEERSCHAUT, A. & GUILLOT-DEUDON, C. (2008): Crystal structure of the new compound $Pb_{3+x}Sb_{3-x}S_{7-x}Cl_{1+x}$ ($x \approx 0.45$). The homologous series $Pb_{(2+2N)}(Sb,Pb)_{(2+2N)}S_{(2+2N)}(S,Cl)_{(4+2N)}Cl_N$ and its perchalcogenide derivatives (N = 1 to 3). *J. Solid State Chem.* **181**, 920-934.

DUCHESNE, J.-C., ROUHART, A., SCHOUMACHER, C. & DILLEN, H. (1983): Thallium, nickel, cobalt and other trace elements in iron sulfides from Belgian lead–zinc vein deposits. *Mineral. Deposita* **18**, 303-313.

ENGEL, P. & NOWACKI, W. (1969): Die Kristallstruktur von Baumhauerit. *Z. Kristallogr.* **129**, 178-202.

FAURE, G. (1991): *Principles and Applications of Inorganic Geochemistry*. Macmillan Publ. Co., New York, N.Y.

GASSER, U. & THEIN, J. (1977): Das syngenetische Sulfidlager Meggen im Sauerland (Struktur, Geochemie, Sekundardispersion). *Forschungsbericht des Landes Nordrhein-Westfalen No. 2630/Fachgruppe Chemie. Westdeutscher.*

GRAESER, S. & EDENHARTER, A. (1997): Jentschite (TlPb As_2SbS_6) – a new sulphosalt mineral from Lengenbach, Binntal (Switzerland).*Mineral. Mag.* **61**, 131-137.

GRAESER, S. & SCHWANDER, H. (1992): Edenharterite (TlPb As_3S_6): a new mineral from Lengenbach, Binntal (Switzerland). *Eur. J. Mineral.* **4**, 1265-1270.

HOFMANN, B.A. & KNILL, M.D. (1996): Geochemistry and genesis of the Lengenbach Pb–Zn–As–Tl–Ba-mineralisation, Binn Valley, Switzerland. *Mineral. Deposita* **31**, 319-339.

JAMBOR, J.L. (1967): New lead sulfantimonides from Madoc, Ontario. 2. Mineral descriptions. *Can. Mineral.* **9**, 191-213.

JOHAN, Z. & MANTIENNE, J. (2000): Thallium-rich mineralization at Jas Roux, Hautes-Alpes, France: a complex epithermal, sediment-hosted, ore-forming system. *J. Czech Geol. Soc.* **45**, 63-77.

JOHAN, Z., MANTIENNE, J. & PICOT, P. (1981): La chabournéite, un nouveau minéral thallifère. *Bull. Minéral.* **104**, 10-15.

KRAUS, W. & NOLZE, G. (2000): POWDERCELL 2.3. Bundesanstalt für Materialforschung und –prüfung, Berlin, Germany.

LAROUSSI, A., MOËLO, Y., OHNENSTETTER, D. & GINDEROW, D. (1989): Argent et thallium dans les sulfosels de la série de la sartorite (gisement de Lengenbach, vallée de Binn, Suisse). *C.R. Acad. Sci. Paris* **308**, *Sér.* II, 927-933.

LE BIHAN, M.-T. (1962): Etude structurale de quelques sulfures de plomb et d'arsenic naturels du gisement de Binn. *Bull. Soc. fr. Minéral. Cristallogr.* **85**, 15-47.

MAKOVICKY, E. (1985): The building principles and classification of sulphosalts based on the SnS archetype. *Fortschr. Mineral.* **63**, 45-89.

MAKOVICKY, E. (1997): Modular crystal chemistry of sulphosalts and other complex sulphides. *In* Modular Aspects of Minerals (S. Merlino, ed.). *Eur. Mineral. Union, Notes in Mineralogy* **1**, 237-271.

MARUMO, F. & NOWACKI, W. (1965): The crystal structure of rathite I. *Z. Kristallogr.* **122**, 433-456.

MARUMO, F. & NOWACKI, W. (1967): The crystal structure of hatchite, $PbTlAgAs_2S_5$. *Z. Kristallogr.* **125**, 249-265.

MATSUSHITA, Y. & TAKÉUCHI, Y. (1994): Refinement of the crystal structure of hutchinsonite, $TlPbAs_3S_9$. *Z. Kristallogr.* **209**, 475-478.

MELLINI, M., MERLINO, S. & ORLANDI, P. (1979): Versiliaite and apuanite, two new minerals from the Apuan Alps, Italy. *Am. Mineral.* **64**, 1230-1234.

MOËLO, Y., MAKOVICKY, E., MOZGOVA, N.N., JAMBOR, J.L., COOK, N., PRING., A., PAAR, W.H., NICKEL, E.H., GRAESER, S., KARUP-MØLLER, S., BALIĆ-ŽUNIĆ, T., MUMME, W.G., VURRO, F., TOPA, D., BINDI, L., BENTE, K. & SHIMIZU, M. (2008): Sulfosalt systematics: a review. Report of the sulfosalt sub-committee of the IMA Commission on Ore Mineralogy. *Eur. J. Mineral.* **20**, 7-46.

MOËLO, Y., ORLANDI, P., GUILLOT-DEUDON, C., BIAGIONI, C., PAAR, W. & EVAIN, M. (2011): Lead–antimony sulfosalts from Tuscany (Italy). XI. The new mineral species parasterryite, $Ag_4Pb_{20}(Sb_{14.5}As_{9.5})_{\Sigma 24}S_{58}$, and associated sterryite, $Cu(Ag,Cu)_3Pb_{19}(Sb,As)_{\Sigma 22}S_{56}$, from the Pollone mine, Tuscany, Italy. *Can. Mineral.* **49**, 623-638.

NESTOLA, F., GUASTONI, A., BINDI, L. & SECCO, L. (2009): Dalnegroite, $Tl_{5-x}Pb_{2x}(As,Sb)_{21-x}S_{34}$, a new thallium sulphosalt from Lengenbach quarry, Binntal, Switzerland. *Mineral. Mag.* **73**, 1027-1032.

ORBERGER, B. (1985): *Les gisements de barytine–pyrite–oxydes de fer de la région de S. Anna* (*Alpes Apuanes, Toscane, Italie*). Doctoral thesis, University of Nancy, Nancy, France.

PANDELI, E., BAGNOLI, P. & NEGRI, M. (2004): The Fornovolasco schists of the Apuan Alps (northern Tuscany, Italy): a new hypothesis for their stratigraphic setting. *Boll. Soc. Geol. Ital.* **123**, 53-66.

PICOT, P. & JOHAN, Z. (1977): *Atlas des minéraux métalliques*. Bur. Rech. Géol. Minières, Mém. **90**.

PRING, A. (2001): The crystal chemistry of the sartorite group minerals from Lengenbach, Binntal, Switzerland – a HRTEM study. *Schweiz. Mineral. Petrogr. Mitt.* **81**, 69-87.

PRING, A., BIRCH, W.D., SEWELL, D., GRAESER, S., EDENHARTER, A. & CRIDDLE, A. (1990): Baumhauerite-2*a*: a silver-bearing minerals with a baumhauerite-like supercell from Lengenbach, Switzerland. *Am. Mineral.* **75**, 915-922.

PRING, A. & GRAESER, S. (1994): Polytypism in baumhauerite. *Am. Mineral.* **79**, 302-307.

REIMANN, C. & DE CARITAT, P. (1998): *Chemical Elements in the Environments. Factsheets for the Geochemist and Enviromental Scientist*. Springer-Verlag, Heidelberg, Germany.

SAWADA, H., KAWADA, I., HELLNER, E. & TOKONAMI, M. (1987): The crystal structure of senandorite (andorite VI): $PbAgSb_3S_6$. *Z. Kristallogr.* **180**, 141-150.

SHELDRICK, G.M. (2008): A short history of SHELX. *Acta Crystallogr.* **A64**, 112-122.

TAKÉUCHI, Y., OHMASA, M. & NOWACKI, W. (1968): The crystal structure of wallisite, $PbTlCuAs_2S_5$, the Cu analogue of hatchite, $PbTlAgAs_2S_5$. *Z. Kristallogr.* **127**, 349-365.

XIONG, Y. (2007): Hydrothermal thallium mineralization up to 300°C: a thermodynamic approach. *Ore Geol. Rev.* **32**, 291-313.

Received April 9, 2011, revised manuscript accepted March 15, 2012.